ACCOUNTS
of chemical research

Review of Chemical Vapor Deposition of Graphene and Related Applications

YI ZHANG,[†,‡,∥] LUYAO ZHANG,[†,§,∥] AND CHONGWU ZHOU*[,†,‡,§]

[†]*Department of Electrical Engineering,* [‡]*Department of Chemistry, and* [§]*Department of Chemical Engineering and Materials Science, University of Southern California, Los Angeles, California 90089, United States*

RECEIVED ON JULY 11, 2012

CONSPECTUS

Since its debut in 2004, graphene has attracted enormous interest because of its unique properties. Chemical vapor deposition (CVD) has emerged as an important method for the preparation and production of graphene for various applications since the method was first reported in 2008/2009. In this Account, we review graphene CVD on various metal substrates with an emphasis on Ni and Cu. In addition, we discuss important and representative applications of graphene formed by CVD, including as flexible transparent conductors for organic photovoltaic cells and in field effect transistors.

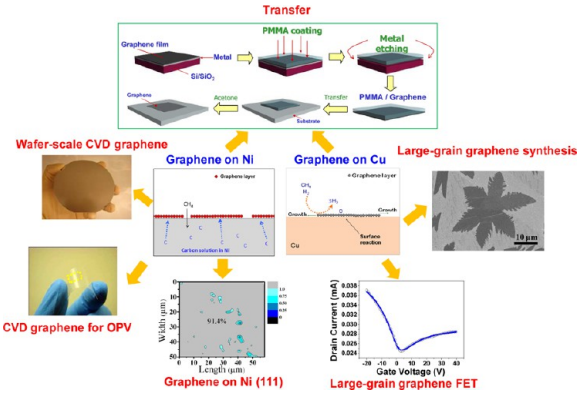

Growth on polycrystalline Ni films leads to both monolayer and few-layer graphene with multiple layers because of the grain boundaries on Ni films. We can greatly increase the percentage of monolayer graphene by using single-crystalline Ni(111) substrates, which have smooth surface and no grain boundaries. Due to the extremely low solubility of carbon in Cu, Cu has emerged as an even better catalyst for the growth of monolayer graphene with a high percentage of single layers. The growth of graphene on Cu is a surface reaction. As a result, only one layer of graphene can form on a Cu surface, in contrast with Ni, where more than one layer can form through carbon segregation and precipitation. We also describe a method for transferring graphene sheets from the metal using polymethyl methacrylate (PMMA).

CVD graphene has electronic properties that are potentially valuable in a number of applications. For example, few-layer graphene grown on Ni can function as flexible transparent conductive electrodes for organic photovoltaic cells. In addition, because we can synthesize large-grain graphene on Cu foil, such large-grain graphene has electronic properties suitable for use in field effect transistors.

Graphene is a two-dimensional material with honeycomb structure. Its unique physical, mechanical, and electrical properties have drawn a lot of interest among scientists.[1−4] Due to the importance and excitement of graphene, a number of review papers have appeared in literature.[4−13] For instance, Geim[4,5] and Fuhrer et al.[6] presented general reviews about graphene and discussed the status and prospects of the graphene field with great insight. In addition, several other review papers have covered specific aspects of graphene properties and applications, such as electronic properties,[7] graphene transistors,[8] graphene photonics and optoelectronics,[9] applications of graphene in energy production and storage,[10] and biosensing applications.[11] Furthermore, chemical exfoliation methods for the production of graphene have also been reviewed by Park and Ruoff.[12] While graphene can be prepared using mechanical exfoliation,[1] epitaxial growth on SiC,[14,15] and chemical exfoliation,[16] chemical vapor deposition (CVD) has emerged as an important method for the preparation and production of graphene since it was first reported in 2008 and 2009.[17−21] However, graphene CVD has not been adequately covered in reviews. As an example, the review by Mattevi et al. was dedicated to CVD of graphene on copper and did not include discussion of CVD graphene

Published on the Web 03/12/2013 www.pubs.acs.org/accounts
10.1021/ar300203n

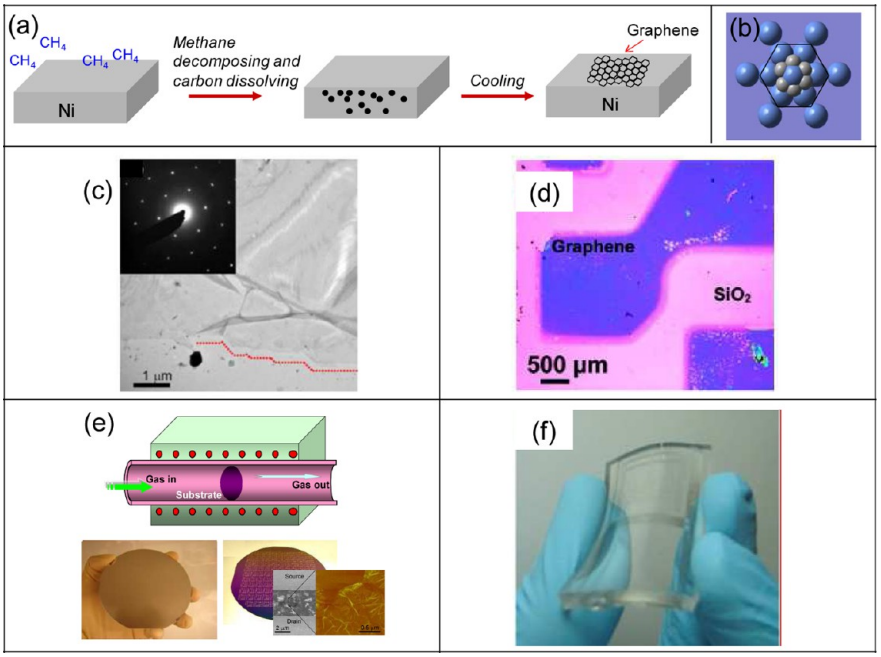

FIGURE 1. (a) Schematic diagram of graphene formation on Ni. (b) Schematic diagram of graphene atoms (smaller atoms) on Ni (111) lattice (larger atoms). (c) Low magnification TEM image of graphene edges (adapted from ref 17). (d) Optical image of graphene transferred from the Ni surface to SiO_2/Si substrate (Adapted with permission from ref 19. Copyright 2009 American Chemical Society). (e) Full-wafer scale deposition of graphene layers on polycrystalline Ni (adapted from ref 18). (f) Transparent and flexible graphene films on the PDMS substrates (adapted from ref 20).

applications.[13] Here we will present a review of graphene CVD on Ni, Cu, and other substrates. In addition, we will review some important and representative applications of CVD graphene, including the use of graphene as flexible transparent conductors for organic photovoltaic (OPV) cells and the use of graphene for field effect transistors (FETs). We will first discuss the chemical vapor deposition of few-layer graphene on polycrystalline Ni film and single crystalline Ni (111) film, and then review the synthesis of single-layer graphene film on Cu. We will further discuss the difference between the graphene growth mechanisms on Ni and Cu, and explain why Cu works better for single-layer graphene synthesis. This will be followed by discussion of selected CVD graphene applications.

Among all the strategies to produce graphene, chemical vapor deposition on transition metal substrates has become the most promising approach, which is inexpensive and produces large-area graphene. During the CVD process, gas species are fed into the reactor and pass through the hot zone, where hydrocarbon precursors decompose to carbon radicals at the metal substrate surface and then, form single-layer and few-layers graphene. During the reaction, the metal substrate not only works as a catalyst to lower the energy barrier of the reaction, but also determines the graphene deposition mechanism, which ultimately affects the quality of graphene. Graphene CVD was first reported in 2008 and 2009, using Ni and Cu substrates,[17−21] which was followed by an explosion of research activities and publications using a variety of transition metal substrates.[22−26] Here, we will focus on Ni and Cu, which are the two major substrates used for graphene CVD.

CVD Synthesis of Graphene on Ni

In general, polycrystalline Ni films are first annealed in Ar/H_2 atmosphere at 900−1000 °C to increase grain size and then exposed to H_2/CH_4 gas mixture. In this step, hydrocarbon decomposes and carbon atoms dissolve into the Ni film to form a solid solution. Finally, samples are cooled down in argon gas. Compared to Cu, Ni has relatively high carbon solubility at elevated temperatures,[27] and the solubility decreases as temperature goes down. During the cooling down process, carbon atoms diffuse out from the Ni−C solid solution and precipitate on the Ni surface to form graphene films. This process is illustrated in Figure 1a. Since Ni(111) has a lattice similar to the densely packed hexagonal lattice of graphene (Figure 1b) and they also have similar lattice constants,[28] Ni surface can serve as an excellent lattice-matched substrate for graphene growth.

Since the graphene growth on Ni is a carbon segregation and precipitation process, different segregation behavior is

produced by different cooling rates, which strongly affect the thickness and quality of graphene films.[17] Medium cooling rates are found to lead to optimal carbon segregation and produce few layer graphene.[17] Besides the cooling rates, microstructure of Ni films also plays an important role in the formation of the graphene film morphology.[17−19] Graphene films grown on Ni substrates are usually continuous with monolayer and few-layers regions. Most of the multilayer nucleation occurs at Ni grain boundaries which are defects in the polycrystalline Ni substrates. It is believed that annealing of Ni substrates at elevated temperatures in hydrogen atmosphere not only increases single-crystalline Ni grain size but also eliminates certain impurities in Ni, therefore improving the graphene quality.[17] In addition, the growth time and hydrocarbon concentration may also affect the graphene thickness due to different amounts of carbon dissolved in Ni films. The specific growth parameters used by several groups are summarized in Table 1.

After synthesis, the as-grown graphene can be transferred to other insulator substrates for further characterization and applications. Figure 1c, taken from ref 17, is a low-magnification transmission electron microscopy (TEM) image of transferred graphene with step-shaped edges. The inset shows the selected area electron diffraction (SAED) pattern of the graphene film along the [001] direction, which confirms the graphene lattice structure. Kong et al. also patterned Ni films to desired geometries to control the graphene growth at particular positions.[19] After transfer to insulator substrates, the geometry can be retained, as Figure 1d shows. Under optimal growth parameters, graphene growth area is only limited by Ni catalyst. Figure 1e shows the wafer-scale graphene synthesis on evaporated Ni films demonstrated by our group.[18] Moreover, the capability of transferring graphene to flexible and transparent substrate demonstrated by Hong et al. allows numerous applications in large-scale flexible transparent electronics (Figure 1f).[20]

Though polycrystalline Ni is a good substrate for graphene synthesis, the percentage and size of monolayer graphene region are still limited by the quality of Ni films, especially the grain size of polycrystalline Ni after thermal annealing. In order to improve the graphene uniformity, single-crystalline Ni(111) substrate with a smooth surface (Figure 2a) is used for graphene growth. The result is compared with polycrystalline Ni with many grain boundaries (Figure 2d).[29] The optical image of as-grown graphene on Ni(111) shows a smooth surface with relatively uniform color (Figure 2b), while the optical image in Figure 2e shows

TABLE 1. Graphene CVD Recipes on Ni Films

ref	Ni film	preannealing condition	growth condition	cooling condition	no. of graphene layers
17	polycrystalline Ni foils, thickness = 0.5 mm, purity > 99.99%	1 h at 1000 °C in H_2	CH_4 = 15 sccm, H_2 = 100 sccm, Ar = 200 sccm; pressure = 1 atm, time = 20 min, temperature = 1000 °C	cooling rate: fast = 20 °C/s, medium = 10 °C/s, slow = 0.1 °C/s	3−4 layers
19	evaporated Ni film on SiO_2/Si substrate, thickness = 500 nm	10−20 min at 900−1000 °C in 600 sccm Ar and 500 sccm H_2	CH_4 = 5−25 sccm, H_2 = 1500 sccm, pressure = 1 atm, time = 5−10 min, temperature = 900−1000 °C		1−12 layers, single/bilayer region up to 20 μm
18	evaporated Ni film on SiO_2/Si substrate thickness=100 nm	800 °C in a Ar/H_2 =10:1 mixture heating and cooling rates 0.15 °C/min	CH_4 = 100 sccm, H_2 = 600 sccm, pressure = 1 atm, time = 8 min, temperature = 800 °C		2−3 layers
20	evaporated Ni film on SiO_2/Si substrate, thickness = 300 nm	1000 °C in Ar	CH_4 = 550 sccm, H_2 = 65 sccm, Ar = 200 sccm, time = 7 min, temperature = 1000 °C	cooling rate: ~10 °C/s in Ar	predominantly mono- and bilayer
50	polycrystalline Ni films evaporated on SiO_2/Si with ~2.6 at % C in the bulk, thickness = 200 nm	1100 °C in vacuum	pressure = 0.4−4 × 10^{-3} Pa, time = 0−100 min, temperature = 1100 °C	cooling rate: 2−50 °C/min	mono- or bilayer graphene up to 95%

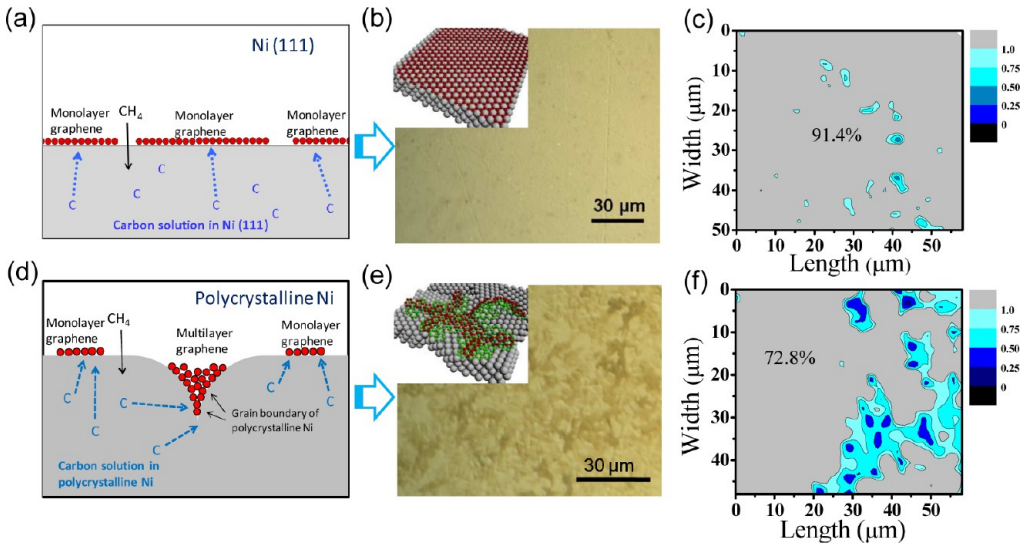

FIGURE 2. Schematic diagrams of graphene growth mechanism on Ni(111) (a) and polycrystalline Ni surface (d). Optical image of graphene grown on Ni(111) (b) and polycrystalline Ni (e). Maps of $I_{G'}/I_G$ of Raman spectra collected on the Ni(111) surface (c) and on the polycrystalline Ni surface (f) (Adapted with permission from ref 29. Copyright 2010 American Chemical Society).

a rough surface with many dark grains which indicate multiple graphene layers on polycrystalline Ni. Further characterization using micro-Raman surface mapping reveals that the area percentage of monolayer/bilayer graphene for Ni(111) substrate is 91.4% (Figure 2c), much higher than the percentage of 72.8% for polycrystalline Ni (Figure 2f).

CVD Synthesis of Graphene on Cu

Besides nickel, people tried a variety of metal substrates such as Cu,[21] Ru,[22] Ir,[23] Pt,[24] Co,[25,30] Pd,[26] and Re,[31] showing different carbon solubility and catalytic effect. In particular, the original study of high quality single-layer graphene growth on polycrystalline Cu films[21] reported by Ruoff et al. attracted a lot of attention due to advantages such as good control of graphene layers, low cost, and ability to transfer.

In the growth method of Ruoff et al., graphene films were grown on 25 μm thick Cu foils in a hot wall furnace.[21] Initially, Cu foil was first annealed in hydrogen atmosphere at 1000 °C, and then a mixture of H_2/CH_4 was introduced into the system to initiate the graphene growth. After a continuous graphene layer was formed on Cu foil, the system was cooled down to room temperature, with results shown in Figure 3 (from ref 21). In Figure 3a, a low magnification SEM image of graphene on a copper substrate clearly shows the Cu grains with color contrast. More details of graphene morphology are revealed in the higher-resolution SEM image (Figure 3b). The Cu surface steps are formed during thermal annealing, and the darker flakes indicate multiple-layer graphene. Graphene "wrinkles" originate

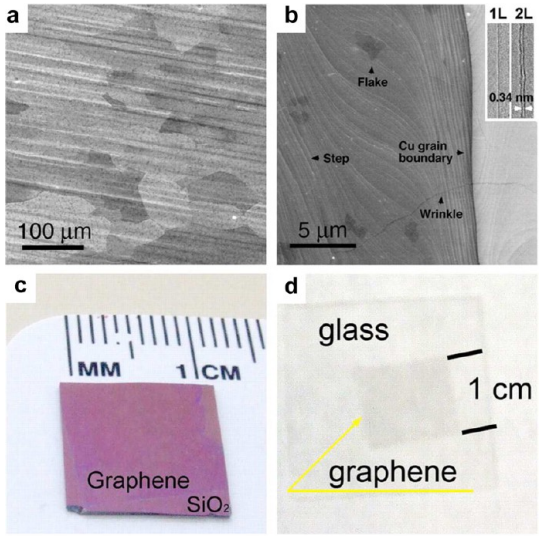

FIGURE 3. (a) SEM image of graphene on a copper foil with growth time of 30 min. (b) High-resolution SEM image of graphene on Cu. Graphene films transferred onto a SiO_2/Si substrate (c) and a glass plate (d). (Adapted from ref 21.)

from the different thermal expansion coefficient of graphene and Cu. Those wrinkles can go across Cu grain boundaries, as Figure 3b shows, indicating that the graphene film is continuous. Graphene grown on Cu foil can be easily transferred to other substrates such as SiO_2/Si and glass (Figure 3c, d) for further evaluation. The optical image analysis over a 1 $\times$ 1 cm^2 region shows predominately monolayer graphene (>95%) with small fractions of bilayer (~3 to 4%) and few-layer (<1%) graphene areas, which is confirmed by Raman spectra.

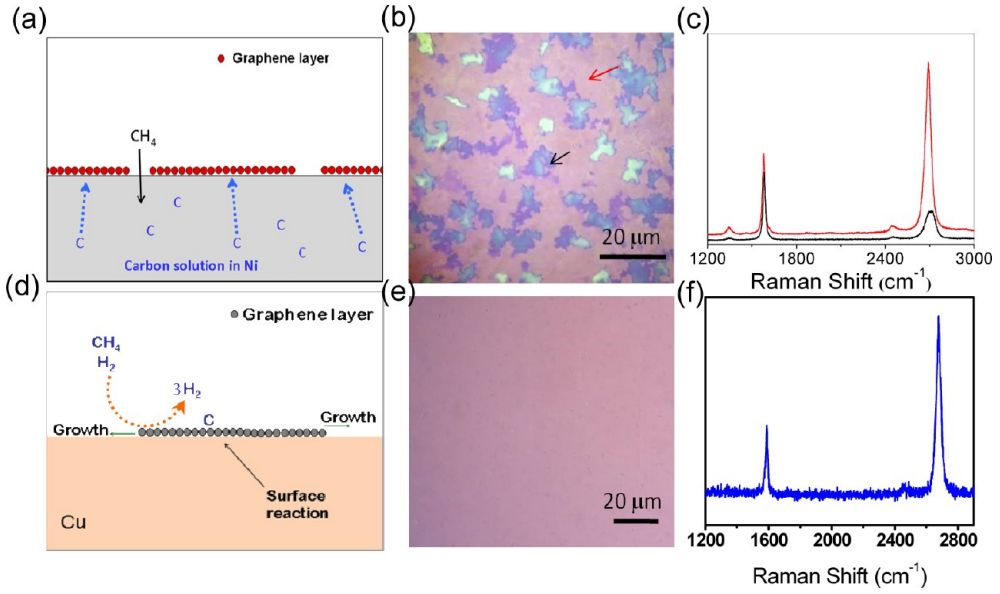

FIGURE 4. Schematic diagrams of graphene growth mechanism on Ni (a) and Cu (d). Optical images of graphene transferred to SiO_2/Si substrates from Ni substrate (b) and Cu substrate (e). Raman spectra collected on graphene synthesized using Ni (c) and Cu (f) substrates.

In our group, we carried out comparative study of graphene growth on Ni and Cu. Compared with graphene growth on Ni, growth parameters such as film thickness and cooling rate have little influence on graphene CVD growth on Cu. The detail comparison is demonstrated in Figure 4. From the optical image of graphene transferred onto SiO_2/Si substrate (Figure 4b), it is obvious that graphene grown on polycrystalline Ni has many multilayer flakes while graphene on polycrystalline Cu is uniform monolayer (Figure 4e), which is also confirmed using Raman spectroscopy (Figure 4c and f). This significant difference suggests different graphene growth mechanisms on Cu and Ni.

For graphene formation on Ni, the growth mechanism has been suggested to be a segregation process (Figure 4a), leading to difficulty in suppression of multilayer formation. In contrast, Cu has ultralow carbon solubility. Even if the hydrocarbon concentration is high or the growth time is long, there is only a small amount of carbon dissolved in Cu. Most of the carbon source for graphene formation is from the hydrocarbon that is catalytically decomposed on the Cu surface (Figure 4d). After the first layer graphene is deposited, Cu surface is fully covered and there is no catalyst exposed to hydrocarbon to promote decomposition and growth. Thus, the graphene growth on Cu is a surface reaction process, which is self-limiting and robust. This mechanism is experimentally proved by using isotopic labeling of hydrocarbon precursors combined with Raman spectroscopic mapping.[32] Recently, various shapes of single-crystal graphene domains such as hexagonal,[33−37] rectangular,[38,39] and flower shape[40−42] with different domain sizes have been achieved by varying growth parameters such as the methane concentration and growth pressure. Some of the growth recipes are summarized in Table 2.

Transfer of Graphene Films

To facilitate graphene for nanoelectronic or photovoltaic applications, we need to remove the catalytic metal substrates from graphene and transfer graphene onto arbitrary substrates. A schematic diagram of the transfer process is shown in Figure 5a. Graphene was first coated by a thin layer of polymethyl methacrylate (PMMA) and then baked at 120 °C to evaporate the solvent. The metal layer was then removed by Ni or Cu etchant, leaving only the PMMA/graphene film. The film is cleaned by deionized (DI) water and then transferred onto a targeting substrate. After evaporating water vapor away, PMMA was removed by acetone, leaving a graphene film on top of the targeting substrate. We were able to transfer both full wafer graphene from Ni film (Figure 5b left) and Cu foil (Figure 5b right) using the above-mentioned method onto glass (Figure 5c), Si/SiO_2 substrates (Figure 5d), and polyethylene terephthalate (PET) films (Figure 5e).

Graphene Photovoltaic Cells

Graphene films are transparent, conductive, and highly flexible, which are considered to be great candidates for transparent conductive electrodes in photovoltaic cells. The conventional OPV cells typically use indium tin oxide (ITO) as

TABLE 2. Graphene CVD Recipes on Cu Films with Different Morphologies

ref	annealing condition	growth condition	graphene morphology	graphene grain size
21	1000 °C in 2 sccm H_2 at 40 mTorr for 20 min	CH_4 = 35 sccm, H_2 = 2 sccm, pressure = 500 mTorr, time = 30 min, temperature = 1000 °C	continuous	
33, 34	1050 °C in 10 sccm H_2 and 300 sccm Ar for 30 min	50 ppm CH_4 in Ar = 300 sccm, H_2 = 20 sccm, pressure = 1 atm, time = 20 min, temperature = 1050 °C	hexagonal structure	~18 μm
39	1045 °C in 50 sccm H_2 and 300 sccm Ar for 3h	CH_4 =0.5 sccm, H_2 = 500 sccm, pressure = 1 atm, time = 15 min, temperature = 1045 °C	regular square with some jagged edges	up to 0.4 × 0.4 mm^2
40		CH_4 = 0.5 sccm and 1.3 sccm, partial pressure = 8 mTorr and 21 mTorr, H_2 = 2 sccm, partial pressure = 27 mTorr, background pressure = 17 mTorr, time = 90 min, temperature = 1035 °C with Cu enclosure	hexagonal symmetry → six-sided polygons → very large graphene domains with growing edges resembling dendrites	up to 0.5 mm
42	1000 °C in 7 sccm H_2at 40 mTorr for 20 min	CH_4 = 2 sccm, H_2 = 25 sccm, pressure = 200 mTorr, time =30 min, temperature = 1000 °C with vapor trapping tube	predominantly six-lobe flowers with four-lobe flowers in some location	~100 μm

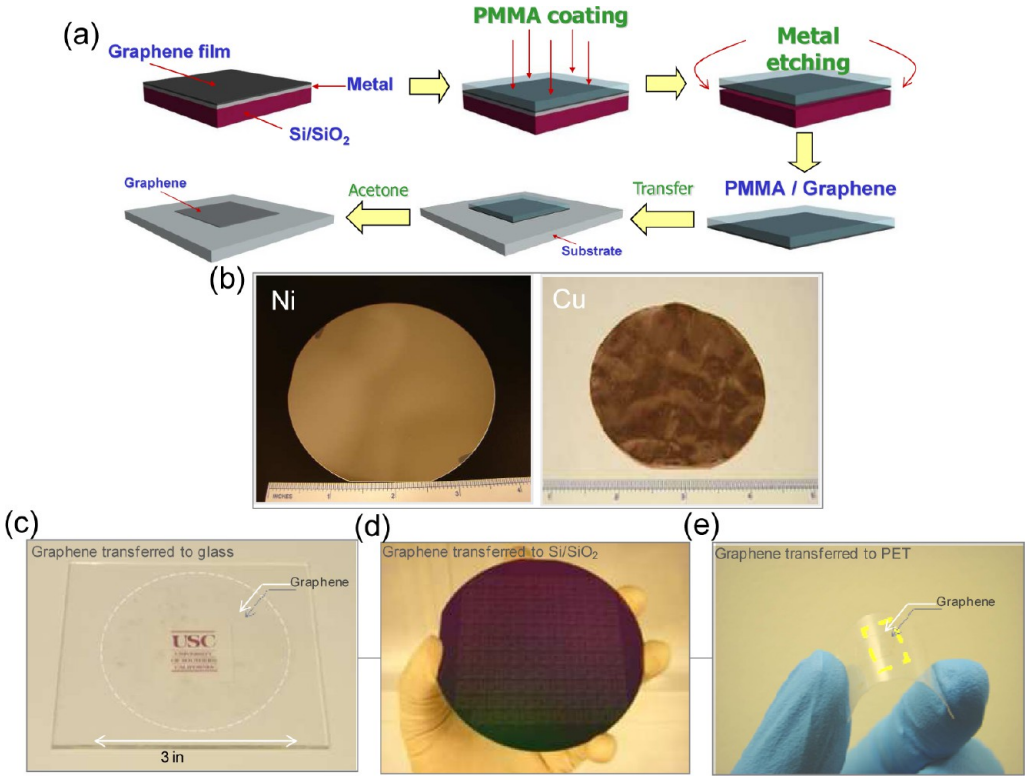

FIGURE 5. (a) Schematic diagram of the transfer process. (b) Wafer-scale synthesis of graphene on evaporated Ni film (left) and Cu foil (right). Graphene films were transferred onto a glass wafer (c), Si/SiO_2 with device patterned (d), and a PET film (e).

anode materials, due to its extremely low sheet resistance (~25 Ω/sq) and high transparency. However, the scarcity of indium reserves and highly brittle nature of metal oxides[43,44] impose serious limitations on the use of ITO for applications where cost, physical conformation, and mechanical flexibility are important.[45] CVD graphene films are highly scalable, transparent (98% transparency for a single-layer graphene film), conductive (hundreds Ω to kΩ/square),

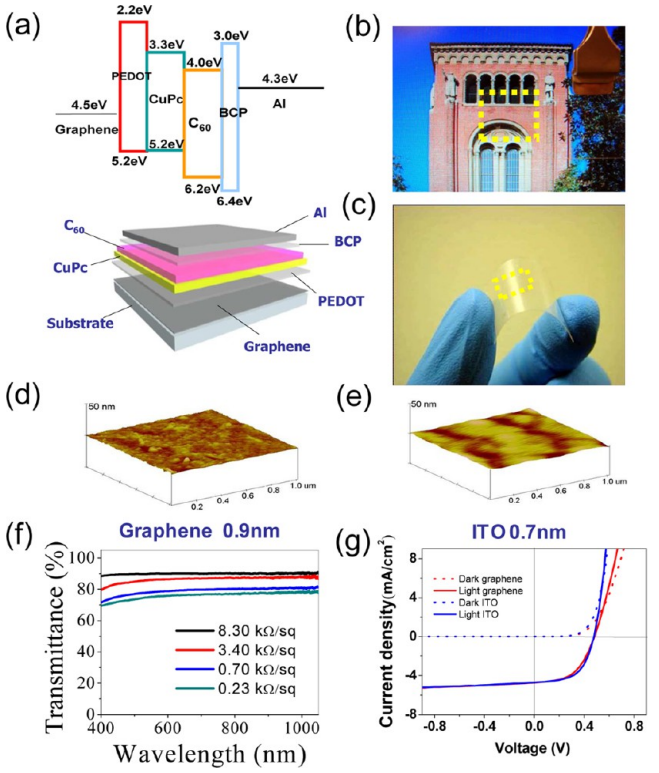

FIGURE 6. (a) Schematic representation of the energy level alignment (top) and construction of the heterojunction organic solar cell fabricated with graphene as anode electrode: CVD graphene/PEDOT/CuPc/C60/BCP/Al. (b, c) Photographs of highly transparent graphene films transferred onto glass (b) and PET (c). (d, e) AFM images of the surface of CVD graphene and ITO, respectively. The scale bar in *z*-direction is 50 nm for both images. (f) Transmission spectra of CVD graphene with different sheet resistance (R_{sheet}). (g) Current density vs voltage characteristics of CVD graphene (red) and ITO (blue) OPV cells on PET under dark (dots) and 100 mW/cm^2 AM1.5G spectral illumination (solid lines) (Adapted with permission from ref 45. Copyright 2010 American Chemical Society).

and cost-effective. Importantly, graphene films are highly flexible and thus are promising for flexible OPV applications.

Few-layer graphene films were used in OPV as anodic materials, as shown in the multilayer structures in Figure 6a. The as-transferred graphene films are highly transparent on both glass and PET as shown in Figure 6b and c, respectively. To obtain good device performance, minimal surface roughness is desirable in order to avoid short circuits and current leakage. Graphene films showed surface roughness of 0.9 nm (Figure 6d), which was comparable with ITO films (0.7 nm in Figure 6e). The sheet resistance and transparency of graphene films could be tuned by controlling the graphene growth process. It is expected that the sheet resistance will decrease when the number of graphene layers increases, but the film transparency will also decrease because of the stacking of graphene layers. Figure 6f shows the above-mentioned trend: while the lowest sheet resistance is 230 Ω/sq with optical transparency of 72%, the highest optical transparency is 91% with sheet resistance of 8.3 kΩ. Therefore, a compromise of sheet resistance and optical transparency should be made to achieve the best performance of the OPV cell.

OPV cells using both graphene on PET and ITO on PET were fabricated and compared side by side. Graphene films were transferred onto PET using the same method shown in Figure 5a. Both graphene/PET and ITO/PET were passivated by spin-coating a layer of poly(3,4-ethylenedioxythiophene)-poly(styrenesulfonate) (PEDOT:PSS) (R_{sheet} = 1 kΩ/sq). PEDOT:PSS was used to mitigate the brittle nature of ITO electrode and improve the rectification behavior of the devices. Figure 6g plots the current density at dark and under illumination for both CVD graphene and ITO cells. Both devices have nearly identical open-circuit voltage (V_{oc}) (for J = 0) of 0.48 V under illumination conditions, which suggests similar recombination behavior in both cells. The $J(V)$ characteristics of the CVD graphene cell under illumination showed a short-circuit photocurrent density (J_{sc}) (for V = 0) of 4.73 mA/cm^2, an open-circuit voltage (V_{oc}) of 0.48 V, and a maximum power (P_{max}) of 1.18 mW/cm^2 to yield a fill factor (FF) of 0.52 and overall power conversion efficiency (η) of 1.18%. In comparison, the ITO/PET control device showed J_{sc} of 4.69 mA/cm^2, V_{oc} of 0.48 V, and P_{max} of 1.27 mW/cm^2 for a FF of 0.57 and an efficiency of 1.27%. Our results reveal that the CVD graphene/PET OPV cell exhibits an output power density nearly 93% of that shown by the ITO cell, although the CVD graphene film has a much higher sheet resistance and lower optical transparency.

The flexibility of graphene OPV cell was tested using bending experiment with an ITO OPV cell as a control. As shown in Figure 7a, the CVD graphene cell performed very well even under 138° bending. In contrast, the ITO cell failed when it was bent at 60° (Figure 7b). Due to the brittle nature of ITO, the illumination loss of ITO device may be related to microcracks induced by bending. The comparison between graphene and ITO devices were further investigated by plotting the fill factor versus the bending angle of both devices (Figure 7c). The fill factor (FF = $P_{max}/J_{sc}V_{oc}$) depends strongly on the output power of the cell and is directly related to the cell conversion efficiency (η) by

$$\eta = \mathrm{FF}\,\frac{J_{sc}V_{oc}}{P_{inc}} \times 100$$

The fill factor dropped slightly from 0.48 to 0.3 with the increase of bending angle from 0° to 138° for the CVD

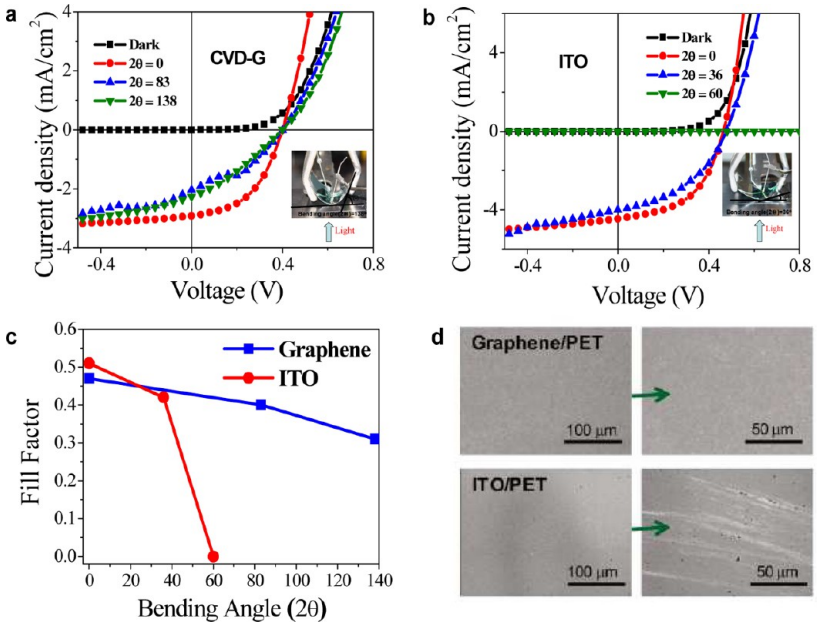

FIGURE 7. (a, b) Current density vs voltage characteristics of CVD graphene (a) and ITO (b) photovoltaic cells under 100 mW/cm^2 AM 1.5G spectral illumination for different bending angles. Insets show the setup employed in the experiments. (c) Fill factor dependence of the bending angle for CVD graphene and ITO devices. (d) SEM images showing the surface structure of CVD graphene (top) and ITO (bottom) photovoltaic cells after being subjected to the bending angles described in panels (a) and (b) (Adapted with permission from ref 45. Copyright 2010 American Chemical Society).

graphene device. In contrast, the fill factor for ITO device dropped dramatically and reached 0 when bent from 0° to 60°. Further SEM characterization of both CVD graphene and ITO surface showed that the CVD graphene film was continuous while the ITO surface had plenty of microcracks after bending. Development of microcracks generated by mechanical stress in ITO, even at small bending angles, can substantially increase the film resistance, which has a key impact in reducing the fill factor. This agrees well with the observed decrease in output current density and power conversion efficiency of the solar cells without observing appreciable change in the V_{oc}. CVD graphene.[45] Overall, CVD graphene has a great advantage over ITO for the use of flexible, transparent, and conductive electrode in OPV cells.

Large-Grain Graphene and Graphene Transistors

Continuous CVD graphene films synthesized on Ni films and Cu foils are usually polycrystalline and with small grain size (several micrometers).[46] As the grain boundaries between each grain of graphene have been found to negatively impact both transport[35,41,47] and mechanical properties,[48] it is therefore of great importance to synthesize large-grain, single-crystalline graphene to facilitate the applications of graphene.

A vapor-trapping method has been developed to synthesize large-grain, single-crystalline graphene.[42] As shown in Figure 8a, Cu foil was loaded into a small half-inch quartz tube and CH_4/H_2 was flown into the large quartz tube (2 in.) for growth. Another piece of Cu foil was loaded into the large quartz tube but outside the half-inch vapor trapping tube as a control. Interestingly, large-grain graphene flowers were found on the Cu foil inside the vapor trapping tube after growth, and the grain size of graphene was up to 100 μm. The SEM images in Figure 6b−d are graphene flowers with different morphology after growth. In comparison, graphene grown on the Cu foil placed outside the vapor trapping tube showed continuous graphene film with slight etching (Figure 8e). The pronounced difference between the two growth results indicates that the vapor trapping tube does play an important role in changing the local environment inside the tube. Reduction of the carbon supply and creation of a quasi-static reactant gas distribution results in large flower-shaped graphene grains. Large-grain graphene flowers were then transferred onto Si/SiO_2 substrate and characterized by micro-Raman microscopy. Figure 8f shows a SEM image of transferred graphene flower on a Si/SiO_2 substrate, and Figure 8g is a corresponding optical microscope image. Three locations were selected for micro-Raman characterization, and the black, red, and blue spectra in Figure 8h correspond to locations A, B, and C in Figure 8g,

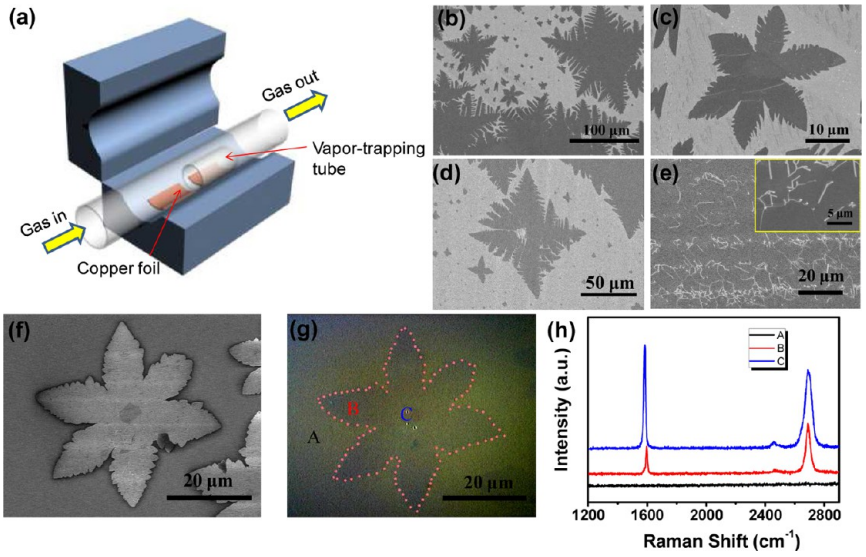

FIGURE 8. (a) Schematic diagram of a vapor-trapping CVD method for graphene growth. (b) Low and (c) high magnification SEM images of a six-lobe graphene flower grown on Cu foil inside the vapor trapping tube. (d) SEM image of a four-lobe graphene flower grown on Cu foil inside the vapor-trapping tube. (e) Graphene grown on Cu foil outside the vapor-trapping tube. (f) SEM image and (g) optical microscope image of a six-lobe graphene flower transferred onto a Si/SiO_2 substrate. (h) Raman spectra taken from location A, B, and C marked in (g) (Adapted with permission from ref 42. Copyright 2012 American Chemical Society).

respectively. The black curve does not show any G or 2D peak, which indicates that no graphene was found outside the graphene flower area. The red curve presents typical features of single-layer graphene: the I_{2D}/I_G intensity ratio is ~0.5, and the full width at half-maximum (fwhm) of the 2D band is ~33 cm^{-1}, which means that the lobes of the graphene flowers are single layer. The I_{2D}/I_G intensity ratio of the blue curve is ~1, and the fwhm of 2D band ~53 cm^{-1}, which represents bilayer graphene in the center of the graphene flower. The large-grain graphene flowers have been confirmed to have single-crystalline lobes and A-B stacking bilayer center using selected area electron diffraction (SEAD).[42]

To investigate the electrical properties of large-grain graphene flowers, field effect transistors (FETs) have been fabricated as shown in Figure 9a. The device shows ambipolar behavior in the plot of drain current (I_{ds}) versus gate voltage (V_g) minus Dirac point voltage (V_{Dirac}) in Figure 9b using D and F as source and drain electrodes. The fitted FET mobility is ~4200 $cm^2\ V^{-1}\ s^{-1}$. The inset of Figure 9b shows that the drain current increases linearly with the increase of drain voltage at different gate voltages, indicating the Ohmic contact between graphene and Pd electrodes. The graphene devices on Si/SiO_2 substrates are not ideal because of the dangling bonds of SiO_2 and charge traps between graphene and SiO_2. To further increase the device mobility, a better dielectric substrate is highly desirable. Hexagonal boron

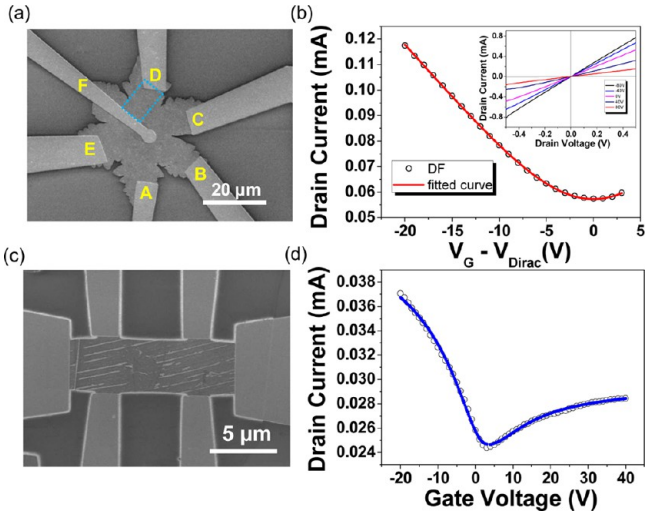

FIGURE 9. (a) SEM image of a six-lobe graphene FET. Electrodes are marked by different letters. The dashed blue square is the region of effective graphene channel between electrode D and F. (b) Plot of drain current (I_{ds}) versus gate voltage (V_g) minus Dirac point voltage (V_{Dirac}) using D and F as source and drain electrodes (black circles) and fitted FET mobility curve (solid red line). Inset is a plot of drain current versus drain voltage at various gate voltages. (c) SEM image of a hall-bar graphene FET on h-BN. (d) Plot of drain current versus gate voltage (Adapted with permission from ref 42. Copyright 2012 American Chemical Society).

nitride (h-BN) is an appealing substrate due to its atomically smooth surface which is relatively free of dangling bonds and charge traps. It also has a lattice constant similar to that of graphite, and has large optical phonon modes and a large

electrical bandgap.[49] Large-grain graphene based hall-bar devices have been fabricated on exfoliated h-BN (Figure 9c). The source-drain voltage is 0.2 V. The plot of drain current (I_{ds}) versus gate voltage (V_g) of graphene device on h-BN shows ambipolar behavior, and the extracted hole and electron mobilities are ~10 000 and ~20 000 $cm^2\ V^{-1}\ s^{-1}$, respectively. The results indicate that large-grain graphene flowers have the advantage over small-grain graphene flakes for the application of high-mobility graphene-based nanoelectronics.

Conclusion

In this Account, we have reviewed the chemical vapor deposition of graphene films on Ni and Cu, and also discussed the difference between the graphene growth mechanisms on Ni and Cu. We also discussed two interesting and important applications achieved by our group, which are multilayer graphene films as flexible, transparent, and conductive anode materials for OPV cells, and large-grain graphene synthesis and its application for field effect transistors on both Si/SiO_2 and h-BN substrates.

In spite of the significant progress reviewed in this Account, there are a number of important and interesting challenges, as discussed below. First of all, synthesizing graphene with large and controlled grain size would be very important for various electronic applications. For instance, is it possible to grow single-grain graphene of centimeter or even wafer scale size? Second, controlling the number of layers and stacking order of graphene is also very important, as bilayer and trilayer graphene may offer functions and properties different from monolayer graphene. In addition, growing graphene directly on insulating substrates such as Si/SiO_2 and h-BN would help to overcome the quality degradation caused by the transfer process. Furthermore, low temperature graphene growth will be attractive to reduce the cost and may enable the direct growth on flexible polymer-based substrates. Last but not least, a deeper understanding of graphene growth chemistry is required. We are convinced that further control and understanding of graphene CVD growth will lead to more breakthroughs in graphene-based nanoscience and nanotechnology.

BIOGRAPHICAL INFORMATION

Yi Zhang received her Ph.D. degree from the University of Southern California in 2012. She had been working in the CVD graphene field for 5 years, and she was among the first to develop full-wafer CVD graphene synthesis and graphene transfer technique. She pioneered the application of CVD graphene for OPV electrodes, as well as the development of large-grain graphene synthesis.

Luyao Zhang received her masters degree from University of California, Los Angeles in 2010. She is now a Ph.D. student in the University of Southern California. She has been working on the CVD graphene field for 3 years.

Chongwu Zhou received his Ph.D. in electrical engineering from Yale University in 1999, and then worked as a postdoctoral research fellow at Stanford University from November 1998 to June 2000. He joined the faculty at University of Southern California in September 2000, and he is a full professor at USC right now. He has authored over 140 journal publications and has won a number of awards, including the NSF CAREER Award, the NASA TGiR Award, the USC Junior Faculty Research Award, and the IEEE Nanotechnology Early Career Award.

FOOTNOTES

*To whom correspondence should be addressed. E-mail: chongwuz@usc.edu.
The authors declare no competing financial interest.
[||]Authors Y.Z. and L.Z. contributed equally to this work.

REFERENCES

1 Novoselov, K. S.; Geim, A. K.; Morozov, S. V.; Jiang, D.; Zhang, Y.; Dubonos, S. V.; Grigorieva, I. V.; Firsov, A. A. Electric Field Effect in Atomically Thin Carbon Films. *Science* **2004**, *306*, 666–669.

2 Novoselov, K. S.; Geim, A. K.; Morozov, S. V.; Jiang, D.; Katsnelson, M. I.; Grigorieva, I. V.; Dubonos, S. V.; Firsov, A. A. Two-Dimensional Gas of Massless Dirac Fermions in Graphene. *Nature* **2005**, *438*, 197–200.

3 Zhang, Y. B.; Tan, Y. W.; Stormer, H. L.; Kim, P. Experimental Observation of the Quantum Hall Effect and Berry's Phase in Graphene. *Nature* **2005**, *438*, 201–204.

4 Geim, A. K.; Novoselov, K. S. The Rise of Graphene. *Nat. Mater.* **2007**, *6*, 183–191.

5 Geim, A. K. Graphene: Status and Prospects. *Science* **2009**, *324*, 1530–1534.

6 Fuhrer, M. S.; Lau, C. N.; MacDonald, A. H. Graphene: Materially Better Carbon. *MRS Bull.* **2010**, *35*, 289–295.

7 Castro Neto, A. H.; Guinea, F.; Peres, N. M. R.; Novoselov, K. S.; Geim, A. K. The Electronic Properties of Graphene. *Rev. Mod. Phys.* **2009**, *81*, 109–162.

8 Schwierz, F. Graphene Transistors. *Nat. Nanotechnol.* **2010**, *5*, 487–496.

9 Bonaccorso, F.; Sun, Z.; Hasan, T.; Ferrari, A. C. Graphene Photonics and Optoelectronics. *Nat. Photonics* **2010**, *4*, 611–622.

10 Brownson, D. A. C.; Kampouris, D. K.; Banks, C. E. An Overview of Graphene in Energy Production and Storage Applications. *J. Power Sources* **2011**, *196*, 4873–4885.

11 Pumera, M. Graphene in Biosensing. *Mater. Today* **2011**, *14*, 308–315.

12 Park, S.; Ruoff, R. S. Chemical Methods For the Production of Graphenes. *Nat. Nanotechnol.* **2009**, *5*, 309–309.

13 Mattevi, C.; Kim, H.; Chhowalla, M. A Review of Chemical Vapour Deposition of Graphene on Copper. *J. Mater. Chem.* **2011**, *21*, 3324–3334.

14 Berger, C.; Song, Z. M.; Li, T. B.; Li, X. B.; Ogbazghi, A. Y.; Feng, R.; Dai, Z. T.; Marchenkov, A. N.; Conrad, E. H.; First, P. N.; de Heer, W. A. Ultrathin Epitaxial Graphite: 2D Electron Gas Properties and a Route Toward Graphene-based Nanoelectronics. *J. Phys. Chem. B* **2004**, *108*, 19912–19916.

15 Berger, C.; Song, Z. M.; Li, X. B.; Wu, X. S.; Brown, N.; Naud, C.; Mayou, D.; Li, T. B.; Hass, J.; Marchenkov, A. N.; Conrad, E. H.; First, P. N.; de Heer, W. A. Electronic Confinement and Coherence in Patterned Epitaxial Graphene. *Science* **2006**, *312*, 1191–1196.

16 Stankovich, S.; Dikin, D. A.; Dommett, G. H. B.; Kohlhaas, K. M.; Zimney, E. J.; Stach, E. A.; Piner, R. D.; Nguyen, S. T.; Ruoff, R. S. Graphene-based Composite Materials. *Nature* **2006**, *442*, 282–286.

17 Yu, Q. K.; Lian, J.; Siriponglert, S.; Li, H.; Chen, Y. P.; Pei, S. S. Graphene Segregated on Ni Surfaces and Transferred to Insulators. *Appl. Phys. Lett.* **2008**, *93*, 113103.

18 De Arco, L. G.; Zhang, Y.; Kumar, A.; Zhou, C. Synthesis, Transfer, and Devices of Single- and Few-Layer Graphene by Chemical Vapor Deposition. *IEEE Trans. Nanotechnol.* **2009**, *8*, 135–138.

19 Reina, A.; Jia, X.; Ho, J.; Nezich, D.; Son, H.; Bulovic, V.; Dresselhaus, M. S.; Kong, J. Large Area, Few-Layer Graphene Films on Arbitrary Substrates by Chemical Vapor Deposition. *Nano Lett.* **2009**, *9*, 30–35.

20 Kim, K. S.; Zhao, Y.; Jang, H.; Lee, S. Y.; Kim, J. M.; Kim, K. S.; Ahn, J.-H.; Kim, P.; Choi, J.-Y.; Hong, B. H. Large-scale Pattern Growth of Graphene Films for Stretchable Transparent Electrodes. *Nature* **2009**, *457*, 706–710.

21 Li, X.; Cai, W.; An, J.; Kim, S.; Nah, J.; Yang, D.; Piner, R.; Velamakanni, A.; Jung, I.; Tutuc, E.; Banerjee, S. K.; Colombo, L.; Ruoff, R. S. Large-Area Synthesis of High-Quality and Uniform Graphene Films on Copper Foils. *Science* **2009**, *324*, 1312–1314.

22 Sutter, P. W.; Flege, J.-I.; Sutter, E. A. Epitaxial Graphene on Ruthenium. *Nat. Mater.* **2008**, *7*, 406–411.

23 Coraux, J.; N'Diaye, A. T.; Busse, C.; Michely, T. Structural Coherency of Graphene on Ir(111). *Nano Lett.* **2008**, *8*, 565–570.

24 Sutter, P.; Sadowski, J. T.; Sutter, E. Graphene on Pt(111): Growth and Substrate Interaction. *Phys. Rev. B* **2009**, *80*, 245411.

25 Varykhalov, A.; Rader, O. Graphene Grown on Co(0001) Films and Islands: Electronic Structure and Its Precise Magnetization Dependence. *Phys. Rev. B* **2009**, *80*, 035437.

26 Kwon, S. Y.; Ciobanu, C. V.; Petrova, V.; Shenoy, V. B.; Bareno, J.; Gambin, V.; Petrov, I.; Kodambaka, S. Growth of Semiconducting Graphene on Palladium. *Nano Lett.* **2009**, *9*, 3985–3990.

27 *ASM Handbook: Alloy Phase Diagrams*; Massalski, T. B.; Okamoto, H.; Subramanian, P. R.; Kacprzak, L., Eds.; ASM International: Materials Park, OH, 2002; Vol. 3.

28 Eizenberg, M.; Blakely, J. M. Carbon Monolayer Phase Condensation on Ni(111). *Surf. Sci.* **1979**, *82*, 228–236.

29 Zhang, Y.; Gomez, L.; Ishikawa, F. N.; Madaria, A.; Ryu, K.; Wang, C.; Badmaev, A.; Zhou, C. Comparison of Graphene Growth on Single-Crystalline and Polycrystalline Ni by Chemical Vapor Deposition. *J. Phys. Chem. Lett.* **2010**, *1*, 3101–3107.

30 Wang, S. M.; Pei, Y. H.; Wang, X.; Wang, H.; Meng, Q. N.; Tian, H. W.; Zheng, X. L.; Zheng, W. T.; Liu, Y. C. Synthesis of Graphene on a Polycrystalline Co Film by Radio-frequency Plasma-enhanced Chemical Vapour Deposition. *J. Phys. D: Appl. Phys.* **2010**, *43*, 455402.

31 Miniussi, E.; Pozzo, M.; Baraldi, A.; Vesselli, E.; Zhan, R. R.; Comelli, G.; Mentes, T. O.; Nino, M. A.; Locatelli, A.; Lizzit, S.; Alfe, D. Thermal Stability of Corrugated Epitaxial Graphene Grown on Re(0001). *Phys. Rev. Lett.* **2011**, 106.

32 Li, X. S.; Cai, W. W.; Colombo, L.; Ruoff, R. S. Evolution of Graphene Growth on Ni and Cu by Carbon Isotope Labeling. *Nano Lett.* **2009**, *9*, 4268–4272.

33 Wu, W.; Jauregui, L. A.; Su, Z.; Liu, Z.; Bao, J.; Chen, Y. P.; Yu, Q. Growth of Single Crystal Graphene Arrays by Locally Controlling Nucleation on Polycrystalline Cu Using Chemical Vapor Deposition. *Adv. Mater.* **2011**, *23*, 4898–4903.

34 Luo, Z.; Kim, S.; Kawamoto, N.; Rappe, A. M.; Johnson, A. T. C. Growth Mechanism of Hexagonal-Shape Graphene Flakes with Zigzag Edges. *ACS Nano* **2011**, *5*, 9154–9160.

35 Yu, Q. K.; Jauregui, L. A.; Wu, W.; Colby, R.; Tian, J. F.; Su, Z. H.; Cao, H. L.; Liu, Z. H.; Pandey, D.; Wei, D. G. Control and Characterization of Individual Grains and Grain Boundaries in Graphene Grown by Chemical Vapour Deposition. *Nat. Mater.* **2011**, *10*, 443–449.

36 Gao, L. B.; Ren, W. C.; Xu, H. L.; Jin, L.; Wang, Z. X.; Ma, T.; Ma, L. P.; Zhang, Z. Y.; Fu, Q.; Peng, L. M.; Bao, X. H.; Cheng, H. M. Repeated Growth and Bubbling Transfer of Graphene With Millimetre-size Single-crystal Grains Using Platinum. *Nat. Commun.* **2012**, *3*, 699.

37 Yan, Z.; Lin, J.; Peng, Z.; Sun, Z.; Zhu, Y.; Li, L.; Xiang, C.; Samuel, E. L.; Kittrell, C.; Tour, J. M. Toward the Synthesis of Wafer-Scale Single-Crystal Graphene on Copper Foils. *ACS Nano* **2012**, *6*, 9110–9117.

38 Wu, Y. A.; Robertson, A. W.; Schaffel, F.; Speller, S. C.; Warner, J. H. Aligned Rectangular Few-Layer Graphene Domains on Copper Surfaces. *Chem. Mater.* **2011**, *23*, 4543–4547.

39 Wang, H.; Wang, G.; Bao, P.; Yang, S.; Zhu, W.; Xie, X.; Zhang, W.-J. Controllable Synthesis of Submillimeter Single-Crystal Monolayer Graphene Domains on Copper Foils by Suppressing Nucleation. *J. Am. Chem. Soc.* **2012**, *134*, 3627–3630.

40 Li, X. S.; Magnuson, C. W.; Venugopal, A.; Tromp, R. M.; Hannon, J. B.; Vogel, E. M.; Colombo, L.; Ruoff, R. S. Large-Area Graphene Single Crystals Grown by Low-Pressure Chemical Vapor Deposition of Methane on Copper. *J. Am. Chem. Soc.* **2011**, *133*, 2816–2819.

41 Li, X. S.; Magnuson, C. W.; Venugopal, A.; An, J. H.; Suk, J. W.; Han, B. Y.; Borysiak, M.; Cai, W. W.; Velamakanni, A.; Zhu, Y. W.; Fu, L. F.; Vogel, E. M.; Voelkl, E.; Colombo, L.; Ruoff, R. S. Graphene Films with Large Domain Size by a Two-Step Chemical Vapor Deposition Process. *Nano Lett.* **2010**, *10*, 4328–4334.

42 Zhang, Y.; Zhang, L. Y.; Kim, P.; Ge, M. Y.; Li, Z.; Zhou, C. Vapor Trapping Growth of Single-Crystalline Graphene Flowers: Synthesis, Morphology, and Electronic Properties. *Nano Lett.* **2012**, *12*, 2810–2816.

43 Scott, J. C.; Kaufman, J. H.; Brock, P. J.; DiPietro, R.; Salem, J.; Goitia, J. A. Degradation and Failure of MEH-PPV Light-Emitting Diodes. *J. Appl. Phys.* **1996**, *79*, 2745–2751.

44 Boehme, M.; Charton, C. Properties of ITO on PET film in Dependence on the Coating Conditions and Thermal Processing. *Surf. Coat. Technol.* **2005**, *200*, 932–935.

45 De Arco, L. G.; Zhang, Y.; Schlenker, C. W.; Ryu, K.; Thompson, M. E.; Zhou, C. W. Continuous, Highly Flexible, and Transparent Graphene Films by Chemical Vapor Deposition for Organic Photovoltaics. *ACS Nano* **2010**, *4*, 2865–2873.

46 Huang, P. Y.; Ruiz-Vargas, C. S.; van der Zande, A. M.; Whitney, W. S.; Levendorf, M. P.; Kevek, J. W.; Garg, S.; Alden, J. S.; Hustedt, C. J.; Zhu, Y.; Park, J.; McEuen, P. L.; Muller, D. A. Grains and Grain Boundaries in Single-Layer Graphene Atomic Patchwork Quilts. *Nature* **2011**, *469*, 389.

47 Yazyev, O. V.; Louie, S. G. Electronic Transport in Polycrystalline Graphene. *Nat. Mater.* **2010**, *9*, 806–809.

48 Shenoy, V. B.; Grantab, R.; Ruoff, R. S. Anomalous Strength Characteristics of Tilt Grain Boundaries in Graphene. *Science* **2010**, *330*, 946–948.

49 Dean, C. R.; Young, A. F.; Meric, I.; Lee, C.; Wang, L.; Sorgenfrei, S.; Watanabe, K.; Taniguchi, T.; Kim, P.; Shepard, K. L.; Hone, J. Boron Nitride Substrates for High-Quality Graphene Electronics. *Nat. Nanotechnol.* **2010**, *5*, 722–726.

50 Liu, N.; Fu, L.; Dai, B. Y.; Yan, K.; Liu, X.; Zhao, R. Q.; Zhang, Y. F.; Liu, Z. F. Universal Segregation Growth Approach to Wafer-Size Graphene from Non-Noble Metals. *Nano Lett.* **2011**, *11*, 297–303.